Eur. J. Biochem. *257*, 449−456 (1998)

Solution conformation of the *Pseudomonas syringae* MSU 16H phytotoxic lipodepsipeptide Pseudomycin A determined by computer simulations using distance geometry and molecular dynamics from NMR data

Vincenza Maria COIRO[1,2], Anna Laura SEGRE[1], Alfredo DI NOLA[2], Maurizio PACI[3], Alessandro GROTTESI[3], Gianluigi VEGLIA[2] and Alessandro BALLIO[4]

[1] Istituto di Strutturistica Chimica 'G. Giacomello', CNR, Montelibretti, Rome, Italy
[2] Dipartimento di Chimica, Università di Roma 'La Sapienza', Rome, Italy
[3] Dipartimento di Scienze e Tecnologie Chimiche, Università di Roma 'Tor Vergata', Rome, Italy
[4] Dipartimento di Scienze Biochimiche 'A. Rossi Fanelli' and Centro di Biologia Molecolare del CNR, Università di Roma 'La Sapienza', Rome, Italy

(Received 27 March/5 May 1998) − EJB 98 0419/3

Pseudomycin A is a cyclic lipodepsinonapeptide phytotoxin produced by a strain of the plant pathogenic bacterium *Pseudomonas syringae*. Like other members of this family of bacterial metabolites, it is characterised by a fatty acylated cyclic peptide with mixed chirality and lactonic closure. Several biological activities of Pseudomycin A are lower than those found for some of its congeners, a difference which might depend on the diverse number and distribution of charged residues in the peptide moiety. Hence, it was of interest to investigate its conformation in solution. After the complete interpretation of the two-dimensional NMR spectra, NOE data were obtained and the structure was determined by computer simulations, applying distance geometry and molecular dynamics procedures. The conformation of the large ring of Pseudomycin A in solution includes three rigid structural regions interrupted by three short flexible regions that act as hinges. The overall three-dimensional structure of the cyclic moiety is similar to that of previously studied bioactive lipodepsinonapeptides produced by other pseudomonads.

Keywords: lipodepsinonapeptide; molecular dynamics; NMR; *Pseudomonas syringae*; Pseudomycin A; solution structure.

Pseudomycin A is the major component of a family of antimycotic lipodepsipeptides isolated from cultures of *Pseudomonas syringae* MSU 16H (Harrison et al., 1991), a bacterium proposed for the biocontrol of *Ophiostoma (Ceratocystis) ulmi*, the causal agent of the highly destructive Dutch elm disease (Lam et al., 1987). Recently, the covalent structure of this bacterial metabolite, including the chirality of amino acid residues (Ballio et al., 1994a), and some of its biological activities (Di Giorgio et al., 1997) have been reported. Pseudomycin A, as well as its congeners Pseudomycin B, Pseudomycin C and Pseudomycin C′, belongs to the group of pseudomonads lipodepsinonapeptides which includes Syringomycins (Segre et al., 1989; Fukuchi et al., 1990a), Syringotoxins (Ballio et al., 1990; Fukuchi et al., 1990b) and Syringostatins (Isogai et al., 1990). At variance with the latter metabolites, the pseudomycins contain an aspartate residue and a lysine residue in the peptide moiety, features which might influence their conformation and biological properties. A comparison between the activities of Pseudomycin A and Syringomycin E, the prototype of pseudomonad lipodepsinonapeptides, in a number of *in vivo* and *in vitro* biological tests has shown that, in general, the efficiency of Pseudomycin A is lower than that of Syringomycin E (Di Giorgio et al., 1997).

As a further step towards the complete molecular characterisation of Pseudomycin A, its solution conformation has been investigated by NMR and computer simulation, applying distance geometry (DG) and molecular dynamics (MD) procedures from NMR and NOE spectroscopy data, after the complete assignment of the NMR spectrum.

A similar approach yielded conclusive information on the structure of the lipodepsinonapeptides white line inducing principle (WLIP) (Mortishire-Smith et al., 1991) and Syringotoxin (Ballio et al., 1994b) and of the eicosipentapeptide Syringopeptin 25A (Ballio et al., 1995).

MATERIALS AND METHODS

NMR spectroscopy. Samples for NMR studies were prepared by dissolving about 1 mg lyophilised sample in 0.8 ml of either D_2O or H_2O/D_2O (9:1, by vol.). NMR spectra of Pseudomycin A were run at 27 °C on a Bruker AMX600 instrument.

Two-dimensional NMR experiments were performed in the phase-sensitive mode with a TPPI (time proportional phase increment) phase cycle (Marion and Wüthrich, 1983) typically using 1 K of memory for 512 increments.

Correspondence to V. M. Coiro, Dipartimento di Chimica, Università di Roma 'La Sapienza', p.le Aldo Moro 5, I-00185 Rome, Italy
Fax: +39 6 490324.
E-mail: coiro@monet.chem.uniroma1.it

Abbreviations. A_2bu, 2,4-diaminobutyric acid; Asp(OH), 3-hydroxyaspartic acid; 2D, two-dimensional; DG, distance geometry; *allo*-Thr, *allo*-threonine; Dhb, (*Z*)-2,3-dehydro-2-aminobutanoic acid; NOE, nuclear Overhauser effect; MD, molecular dynamics; Thr(Cl), 4-chlorothreonine; TPPI, time proportional phase increment; SA, simulated annealing; WLIP, white line inducing principle.

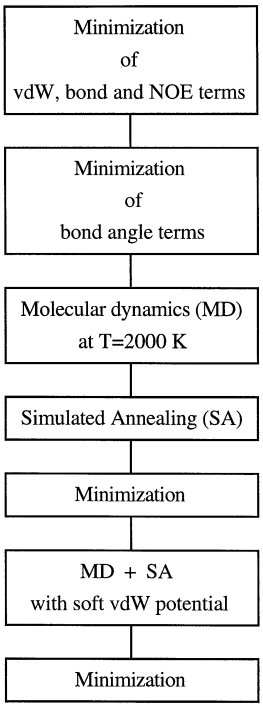

Fig. 1. Flowchart of the distance-geometry–simulated-annealing protocol.

Zero filling was used to obtain a 1 K×1 K real matrix. The number of scans was optimised in order to obtain a satisfactory signal/noise ratio.

Correlation experiments were performed using total correlation experiments (TOCSY), with the spinlock composite pulse sequence inserted (Braunschweiler and Ernst, 1983) and a typical mixing time of 0.080 s in order to observe both direct and remote connectivities. The mixing time for the NOE magnetisation exchange was 0.080 s.

Data were processed with Bruker two-dimensional NMR software. Free induction decays were weighted by a sinebell apodisation function shifted typically $\pi/3$ in both dimensions.

A baseline correction was carried out in both dimensions using a polynomial fit routine present in the same program.

Computer simulations. The search for the structure that accounts for the experimental NOEs was performed by distance geometry−simulated annealing (DG−SA) and molecular dynamics (MD) simulations.

Distance-geometry−simulated annealing procedure. DG−SA, energy minimisation and the subsequent analysis of the structures were performed using the standard X-PLOR 3.1 version (Brünger, 1988). The calculations were based on the hybrid distance geometry−simulated annealing protocol (Kirkpatrick et al., 1983; Wagner et al., 1987; Nilges et al., 1988) using the force field included in X-PLOR for DG−SA calculations. Further refinements were performed with the CHARMM empirical energy function (Brooks et al., 1983a; MacKerell et al., 1992). Distances estimated from 2D NOESY spectra were classified into three groups as strong, medium or weak and given upper bounds of 0.32, 0.40 and 0.50 nm, respectively (Kaptein et al., 1988). For prochiral methylene or methyl groups, pseudoatoms were used and an additional distance term of 0.05 nm was added to the upper distance bounds.

The peptidic torsion angles were restrained in *trans* conformation by adding a proper dihedral potential. A restraining potential for χ angle of the 2,3-dehydro-2-aminobutanoic (Dhb) residue was included to maintain the *Z* conformation.

The procedure proposed by Nilges et al. (1988) was used, as described in Fig. 1. We used 100 cycles of Powell minimisation (Powell, 1977) of van der Waals, bond and NOE terms and 100 subsequent cycles of the bond angle terms to improve the covalent geometry of the embedded structures. This was followed by a molecular dynamics simulation stage, starting at a temperature of 2000 K, to introduce the chirality and planarity. The correct handedness of the structure was established on the basis of the lowest energy of the embedded structures. The subsequent stage was the cooling of the structures to a final temperature of 100 K with increased van der Waals' terms. Finally 200 steps of Powell minimisation of the structures were performed. The obtained structures were then refined by a further simulated annealing stage consisting of 1000 steps of MD calculation at 2000 K and then of 1000 cooling steps to a final temperature of 100 K. The van der Waals' interactions were softened to enable atoms to move through each other. The structures obtained were then subjected to 100 cycles of energy minimisation using the conjugated gradients of Powell algorithm. The criteria of acceptance adopted for the generated structures were: deviation of the actual distance, r_{ij}, from the experimental upper distance, r_{ij}^{+}, determined by the NOE intensity, $r_{ij} \leq r_{ij}^{+} + 0.05$ nm; rms difference for the covalent bond deviations from ideality of < 0.001 nm; rms difference for bond angle deviations from ideality of $< 2°$.

Cluster analysis. The program MacDendro (Thioulouse, 1989) was used for a cluster analysis. The aim of this analysis is to place structures into clusters, such that structures within a given cluster tend to be similar and structures within different clusters tend to be dissimilar. To do this, a non-hierarchical partitioning algorithm was used: a tentative number of clusters (K) is given as input and the initial partition is set at random; the program output gives the best partition of the structures in the number of clusters chosen. Using different K values as input, the best K can be obtained. The algorithm was applied to the distance matrix between all pairs of spatial structures. The distance matrix was obtained as follows: given a set of N structures, for each pair of structures *ij*, the distances between the same backbone atoms in the two structures were calculated and the root mean square r_{ij} of all the distances (rmsd) was obtained. r_{ij} represents the element of the distance matrix, so that each structure is represented by a row of N elements in the matrix and can be represented by a point in an N-dimensional space. Hence, the ensemble of N structures gives rise to a cloud. The cloud can be partitioned into clusters and the quality of the partition can be judged by the inertia ratio R = (between clusters moment)/(total moment); the higher R is, the better the partition. Most of the algorithms used in MacDendro are described by Roux (Roux, 1985).

Energy parameters. The CHARMM force field was used to model the peptide (Brooks et al., 1983b; MacKerell et al., 1992), and the TIP3P model was used for water (Jorgensen et al., 1983). Polar hydrogen atoms were explicitly included in this model and the hydrogen bond was modelled as a purely electrostatic interaction. Electrostatic interactions were truncated on a group basis at a distance of 0.9 nm. A dielectric constant of 1 was used.

Restrained molecular dynamics in vacuo. The calculations were based on an energy function approach: the total energy of the molecule was given by the combination of an empirical and an effective energy term.

$$E_{\text{total}} = E_{\text{empirical}} + E_{\text{effective}}$$

The empirical potential energy function contained terms representing bond angles, dihedrals, improper dihedrals, and van der Waals' and electrostatic interactions.

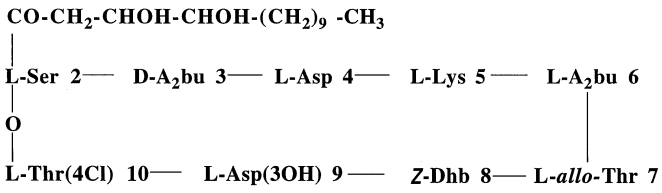

Fig. 2. Primary structure of Pseudomycin A.

The effective energy function for the distance restraints, E_{dist}, used was

$$E_{dist} = k_{dist} \Sigma [r_{ij} - r_{ij}^{+}]^2 \qquad \text{if } r_{ij} > r_{ij}^{+}$$

and

$$E_{dist} = 0 \qquad \text{if } r_{ij} \leq r_{ij}^{+}$$

where r_{ij}^{+} is the upper bound of the distance previously reported and, r_{ij} is the calculated distance; k_{dist} was set at 4186 kJ · mol^{-1} · nm^{-2}. All bond lengths were kept fixed with the SHAKE algorithm (Ryckaert et al., 1977). The temperature of the system was kept constant by weak coupling to a thermal bath (Berendsen et al., 1984). The time step of integration was 2 fs. The MD protocol was the following: after 100 steps of Powell minimisation (Powell, 1977) 30 ps of MD simulation *in vacuo* were performed including the NOE restraints.

Stochastic boundary molecular dynamics. MD simulations in water were carried out with the stochastic boundary method (Brooks and Karplus, 1983; Brooks et al., 1985; Brünger et al., 1985). They included an approximately spherical region centred on the N atom of serine, with a radius of 1.4 nm. The sphere was filled with water molecules, so that a total of 980 water molecules resulted. After termalisation, each simulation was run for 130 ps. The last 100 ps were used for analysis. In these simulations the effective energy function, E_{dist}, was switched off.

RESULTS

The covalent structure of Pseudomycin A is reported in Fig. 2.

NMR spectroscopy. The two-dimensional NMR spectra led to the individual assignment of all residues and the NOEs observed eventually allowed the determination of the conformation in solution. The experiments were performed both in D_2O and in H_2O/D_2O (9:1 by vol.).

The complete assignment of the resonances was achieved by the TOCSY spectrum, which identified all the spin systems of the residues.

Particularly, the resonances present in the olefinic region, with a quartet of 1:3:3:1, could be easily assigned to the protons of the CH groups of the Dhb moiety as found in other lipodepsipeptides (Segre et al., 1989; Ballio et al., 1990, 1991, 1994b).

In the aliphatic region the assignments were based on the direct and remote scalar connectivities in TOCSY experiments and on the chemical shift values reported in the literature (Gross and Kalbitzer, 1988).

The complete assignment of the resonances of the NMR spectrum is given in Table 1.

The fingerprint region of the TOCSY spectrum in H_2O/D_2O (9:1 by vol.) indicated the direct connectivity between the resonances of NH and those of C$^{\alpha}$H protons of the backbone (spectrum not shown). Together with the NOESY spectrum allowed the complete sequential assignment has been obtained.

NOE cross-peaks were observed among resonances and used for the determination of the solution structure of Pseudomycin A. All NOE cross-peaks indicating the through-space proximity observed, are summarised in Table 2, together with an estimate of their relative intensity. The observed NOEs are not homogeneously distributed along the structure. This indicates that there are flexible regions in the molecule which cancel the specific proton−proton magnetisation transfer.

The measure of the dependence on temperature of the chemical shift of the NH amide protons of Pseudomycin A (Table 3) shows that some protons are shielded from solvent accessibility in the chemical exchange. In particular, the rather small temperature coefficient of the NH of A_2bu3, Lys5, *allo*-Thr7, Dhb8 and Asp(OH)9 indicates that they are involved in a hydrogen bond.

Table 1. Chemical shifts and assignment of ^{1}H NMR spectrum.

Residue	δ ppm		Residue	δ ppm	
	Assign.	^{1}H		Assign.	^{1}H
Fat1	2 CH	2.58	Lys5	NH	8.36
	2′ CH	2.53		C$^{\alpha}$H	4.15
	3 CH	3.95		C$^{\beta}$H	2.02
	4 CH	3.63		C$^{\gamma}$H	1.36
	5′ CH	1.63		C$^{\gamma}$H′	1.24
	5 CH	1.57		C$^{\delta}$H	1.71
	6 CH	1.46		C$^{\epsilon}$H	2.99
	6′ CH	1.43			
	7−11 CH	1.35	A_2bu6	NH	9.19
	12 CH	1.35		C$^{\alpha}$H	4.59
	13 CH	1.33		C$^{\beta}$H	2.33
	14 CH	0.90		C$^{\beta}$H′	2.18
				C$^{\gamma}$H	3.15
Ser2	NH	8.90			
	C$^{\alpha}$H	4.76	*allo*-Thr7	NH	8.48
	C$^{\beta}$H	4.39		C$^{\gamma}$H	4.20
				C$^{\beta}$H	4.10
A_2bu3	NH	8.83		C$^{\gamma}$H	1.35
	C$^{\alpha}$H	4.32			
	C$^{\beta}$H	2.25	Dhb8	NH	9.65
	C$^{\gamma}$H	3.22		C$^{\beta}$H	6.87
	C$^{\gamma}$H′	3.15		C$^{\gamma}$H	1.77
Asp4	NH	8.46	Asp(OH)9	NH	7.85
	C$^{\alpha}$H	4.22		C$^{\alpha}$H	5.02
	C$^{\beta}$H	2.73		C$^{\beta}$H	4.83
	C$^{\beta}$H′	2.87			
			Thr(Cl)	NH	8.72
				C$^{\alpha}$H	5.14
				C$^{\beta}$H	4.53
				C$^{\gamma}$H′	3.62
				C$^{\gamma}$H	3.55

Computer simulations. *Distance-geometry-simulated annealing and cluster analysis.* DG-SA computations were performed including in the calculations the NOE restraints obtained by NMR data as reported in the experimental section.

Fifty final structures were generated and the 30 best structures (low NOE violations and low total energies) were retained for further analysis. The cluster analysis showed that the structures could be grouped into two classes: **I** and **II**. The rmsds among the backbone atoms were 0.08 nm and 0.11 nm for classes **I** and **II**, respectively, and the rmsd between the average structures of each class was 0.50 nm. The two clusters are well separated in space. In fact the centroides of the two clusters are 0.76 nm apart; class-**I** cluster is completely contained within a hypersphere of 0.35 nm radius, while class-**II** cluster is contained within a hypersphere of 0.37 nm radius.

Table 2. NMR NOE intensity observed. The relative intensity is reported as s (strong), m (medium) and w (weak) as defined in the experimental part.

Atom pair	Intensity
Intraresidual NOEs	
1) NH Dhb−C$^{\gamma}$H Dhb	(m/s)
2) C$^{\beta}$H Dhb−C$^{\gamma}$H Dhb	(m)
3) NH Asp−C$^{\alpha}$H Asp	(m/s)
4) NH A_2bu6−C$^{\beta}$H A_2bu6	(m/s)
5) NH Asp−C$^{\beta}$H/H′ Asp	(s/m)
6) NH Lys−C$^{\alpha}$H Lys	(s)
7) NH A_2bu3−C$^{\beta}$H A_2bu3	(s)
8) NH Ser−C$^{\alpha}$H Ser	(w)
9) NH Ser−C$^{\beta}$H Ser	(w)
10) NH Asp(OH)−C$^{\alpha}$H Asp(OH)	(w)
11) NH *allo*-Thr−C$^{\alpha}$H *allo*-Thr	(w)
12) NH *allo*-Thr−C$^{\beta}$H *allo*-Thr	(s)
13) NH *allo*-Thr−C$^{\gamma}$H *allo*-Thr	(m/s)
14) NH Lys−C$^{\gamma}$H Lys	(w)
15) NH Lys−C$^{\delta}$H′ Lys	(m/w)
16) NH Lys−C$^{\delta}$H Lys	(w)
Interresidual NOEs	
1) NH Dhb−C$^{\alpha}$H *allo*-Thr	(m)
2) C$^{\alpha}$H *allo*-Thr−NH Asp(OH)	(w)
3) C$^{\alpha}$H Lys−NH A_2bu6	(s)
4) NH Ser−C$^{\alpha}$H Lys	(w)
5) NH Lys−C$^{\alpha}$H Asp	(w)
6) NH A_2bu3−C$^{\alpha}$H Asp	(m)
7) NH A_2bu3−C$^{\beta}$H Ser	(m/w)
8) NH A_2bu3−C$^{\alpha}$H Ser	(m/w)
9) NH Thr(Cl)−C$^{\alpha}$H Ser	(m/w)
10) NH Thr(Cl)−C$^{\alpha}$H Asp(OH)	(s)
11) NH Ser−2 CH Fat	(s)
12) NH Dhb−NH Asp(OH)	(m)
13) NH Lys−NH Asp(OH)	(w)
14) NH A_2bu6−NH *allo*-Thr	(w)
15) NH A_2bu6−NH Lys	(w)
16) NH Thr(Cl)−NH Asp(OH)	(w)
Observed long-range NOEs	
1) C$^{\beta}$H Dhb−C$^{\alpha}$H Ser	(m/s)
2) NH Asp−C$^{\alpha}$H Ser	(w)
3) NH Lys−C$^{\alpha}$H Ser	(m/w)
4) NH Asp(OH)−C$^{\alpha}$H Ser	(m)
5) NH Asp−C$^{\beta}$H A_2bu6	(w)
6) NH Dhb−C$^{\alpha}$H Ser	(w)
7) NH A_2bu3−C$^{\alpha}$H Lys	(w)

Table 3. Chemical shift dependence on temperature of the amide protons.

Residue	$\Delta \pm 0.0025$
	ppm/K
Ser2	0.0125
A_2bu3	0.0013
Asp4	0.0163
Lys5	0.0063
A_2bu6	0.0155
allo-Thr7	0.0038
Dhb8	0.0078
Asp(OH)9	0.0025
Thr(Cl)10	0.0131

Table 4. Structural statistics[a]

Structural parameter	Class **I**[b]	Class **II**[c]
<Backbone atom rmsd to mean>[d] (nm)	0.08 ± 0.03	0.11 ± 0.03
<All heavy atom rmsd to mean> (nm)	0.30 ± 0.06	0.43 ± 0.05
<rmsd from experimental distance restraints>[e] (nm)	0.004 ± 0.001	0.049 ± 0.008
<rmsd from experimental dihedral angle restraint>[e] (°)	0.008 ± 0.020	0.422 ± 0.582
<Overall energy> (kJ/mol)	67 ± 21	109 ± 38

[a] Final refined structures obtained with Full Embed-DGSA protocol. <> indicates average values.
[b] Class **I**: set of 15 converged structures.
[c] Class **II**: set of 15 converged structures.
[d] N, C and C$^{\alpha}$ of amino acid residues, without N of Ser residue.
[e] The rmsds from the experimental restraints are calculated with respect to the upper limit of the distance and dihedral restraints. None of the structures exhibited distance violations greater than 0.03 nm.

It has to be pointed out that the experimental NOE restraints involve mainly the backbone atoms. As a consequence, the structures obtained are more reliable for the backbone than for the side chains.

The structure of each class with the lowest deviation from the average structure was taken as the most representative structure of the class and was used for further MD simulations. Structural statistics for class **I** (15 structures) and class **II** (15 structures) and differences between atomic rmsds are given in Table 4.

Molecular dynamics simulations. The most representative structure of each class was subjected to 30 ps MD simulation *in vacuo* followed by 130 ps MD in water.

The simulations *in vacuo* and in water gave comparable results in terms of the overall shape of the molecule. The main differences were due to a rotation of the dihedral angles involving the Ser2 and the lactone ring closure for class-**I** structure and the Ser2 for class-**II** structure, respectively, and to the presence of the hydrogen bonds. Hereafter we will discuss the results obtained in the last 100 ps of the simulation in water. The average potential energies of the two classes are comparable within one standard deviation, being 1806 ± 64 kJ/mol and 1773 ± 78 kJ/mol, for class **I** and **II**, respectively. The two classes showed a different pattern of hydogen bond network, as reported in Table 5. The chemical shift behaviour of the NH proton resonances, reported in Table 3, can be compared with the hydrogen bonds observed in the MD simulation (Table 5). The NMR results (Table 3) indicate which protons are shielded from solvent and less accessible to exchange dynamics. Table 5 shows that class-**I** structure exhibits three hydrogen bonds with good donoracceptor distance and angle; they are the N A_2bu3−O Fat1, N Asp(OH)9−O Lys5 and N Asp(OH)9−O A_2bu6, respectively. The amidic protons involved have small temperature coefficients. The two other hydrogen bonds of class **I**, N Dhb8−O Lys5 and N A_2bu6−O Asp4, have less favourable angular values (111° and 103°, respectively) and involve amidic protons with intermediate and large temperature coefficients, respectively. Thus, the hydrogen bonds observed in the MD simulations are confirmed by the experimental NMR data. However, the NMR data show that two other amidic protons are involved in (intramolecular) hydrogen bonds: the HN of Lys5 with an intermediate temperature coefficient and the HN of *allo*-Thr7 with a small temperature coefficient. Though they were not involved in

Table 5. Hydrogen bonds detected during the last 100 ps of molecular dynamics simulation in water. Hydrogen bonds common to both classes are marked.

H bond	Donor-acceptor average distance	Average angle	Occurrence time
	nm	degrees	%
Class **I**			
N A_2bu3−O Fat1	0.26	132	70
N A_2bu6−O Asp4	0.28	103	87
• N Dhb8−O Lys5	0.33	111	71
N Asp(OH)9−O Lys5	0.33	148	61
* N Asp(OH)9−O A_2bu6	0.32	137	54
Class **II**			
N Ser2−O Lys5	0.33	100	51
N Asp4−O Ser2	0.28	101	97
N Lys5−O Ser2	0.30	161	91
• N Dhb8−O Lys5	0.32	149	94
* N Asp(OH)9−O A_2bu6	0.26	147	100

Table 6. Distance constraint violations: NOE effects observed in the NOESY spectra. The relative intentisy is reported as strong, medium and weak as defined in the test. (V) Pseudoatom, located at the geometric center of the involved proton positions. An additional 0.05 nm was added to the upper limits of NOESY distance constraints to allow for the use of pseudoatoms.

NMR NOE	NOE intensity	Molecular dynamics average distances (rms fluctuation) for	
		Class **I**	Class **II**
		nm	
HN Ser2−C$^{\alpha}$H Lys5	W	0.62 (0.03)	− −
HN A_2bu3−C$^{\alpha}$H Asp4	M	0.52 (0.02)	0.56 (0.01)
HN Asp4−C$^{\beta}$H A_2bu6	W	− −	(V) 0.71 (0.03)
HN Lys5−HN Asp(OH)9	W	− −	0.62 (0.04)
HN *allo*-Thr7−C$^{\beta}$H *allo*-Thr7	S	− −	0.40 (0.00)
HN A_2bu3−C$^{\alpha}$H Lys5	W	− −	0.65 (0.01)

hydrogen bonds in the simulation in water, they were involved in the simulation in vacuo. In addition, the average donor−acceptor distances N *allo*-Thr7−O Lys5 and N Lys5−O Ser2 and N− H · · · O corresponding angles in water were 0.35 nm and 70° and 0.40 nm and 126°, respectively, thus suggesting that they could be detected by a wider sampling of the conformational space allowed for class **I**, i.e. with a much longer simulation. To speed up the simulation, a new simulation was performed in water at a temperature of 325 K. In this simulation we have observed, with small occurrence, two additional hydrogen bonds: one between the amidic proton of *allo*-Thr7 and the oxygen of Lys5 and one between the amidic proton of Lys5 and the oxygen of Ser2, respectively.

The hydrogen bond pattern of class-**II** structure is different. A comparison of the MD and NMR results shows that the experimental data account for two amidic protons, HN of A_2bu3 and HN of *allo*-Thr7, with small temperature coefficients, not involved in any intramolecular hydrogen bond in the MD simulation in water. MD simulations *in vacuo* and in water at a temperature of 325 K did not show any intramolecular hydrogen bond for these protons.

Table 7. β and γ turns during the last 100 ps of molecular dynamics simulation in water. Averaged dihedral angle values.

Turn	Position $i+1$		Position $i+2$		β-turn type	Occurrence time
	ϕ	ψ	ϕ	ψ		
	degrees					%
Class **I**						
β-turn:						
N Dhb8−O Lys5	52	−150	−66	−27	II′	76
N Asp(OH)9−O A_2bu6	−66	−27	−55	−44	III	54
γ-turn:						
N A_2bu3−O Fat1	67	−69				70
N A_2bu6−O Asp4	61	−95				87
Class **II**						
β-turn:						
N Lys5−O Ser2	67	−100	−85	−15	II′	91
N Dhb8−O Lys5	54	33	37	46	III′	94
N OH-Asp9−O A_2bu6	37	46	71	14	III′	100
γ-turn:						
N Asp4−O Ser2	67	−100				97

It may be concluded that the hydrogen bond pattern exhibited by class-**I** structure corresponds better than that of class-**II** structure to the experimental evidence.

In Table 6 the distance violations which occurred in the simulation are reported. Again, the class-**I** structure shows a better agreement with the experimental data than does that of class **II**.

*Structural analysis of classes **I** and **II***. In Table 7 the secondary structures found in the MD simulation in water are reported (Table 7). The class-**I** structure is characterised by the presence of four consecutive turns. The sequences Fat1−Ser2−A_2bu3 and Asp4−Lys5−A_2bu6 form two γ-turn structures although the ϕ/ψ torsion angles deviate from the usual values, being ϕ_2 and ψ_2 67° and −69° (with rms fluctuations of 4° and 13°) and ϕ_5 and ψ_5 61° and −95° (with rms fluctuations of 7° and 17°), respectively (Rose et al., 1985). A β turn involves the residues Lys5−A_2bu6−*allo*-Thr7−Dhb8, stabilised by a hydrogen bond between CO of Lys5 and NH of Dhb8 with an occurrence time of 76%; it can be defined as type II′ with ϕ_6, ψ_6, ϕ_7 and ψ_7 averaged dihedral angle values of 52°, −150°, −66° and −27° and rms fluctuations of 6°, 17°, 13° and 11°, respectively. Finally, a second β turn involving the residues A_2bu6−*allo*-Thr7−Dhb8−Asp(OH)9, stabilised by a hydrogen bond between CO of A_2bu6 and NH of Asp(OH)9, is present with ϕ_7, ψ_7, ϕ_8 and ψ_8 averaged dihedral angle values of −66°, −27°, −55°, −44° and rms fluctuations of 13°, 11°, 9° and 7°, respectively and an occurrence time of 54%; it can be defined as a type III β-turn (Rose et al., 1985).

Due to the flexibility of the torsion angles involved, a conformational flexibility, in particular of the region from residue 6 to 9, is observed. In Fig. 3a the superposition of the conformations obtained every 4 ps is reported.

The class-**II** structure also has four consecutive turns. The sequences Ser2−A_2bu3−Asp4 forms a γ-turn structure although the ϕ/ψ torsion angles deviate from the usual values, being ϕ_3 and ψ_3 67° and −100° (with rms fluctuations of 5° and 10°), respectively (Rose et al., 1985). A β turn is stabilised by a hydrogen bond between CO of A_2bu6 and NH of Asp(OH)9, with an occurrence time of 100%. The average ϕ/ψ dihedral angles are ϕ_7 = 37°, ψ_7 = 46°, ϕ_8 = 71° and ψ_8 = 14° with rms

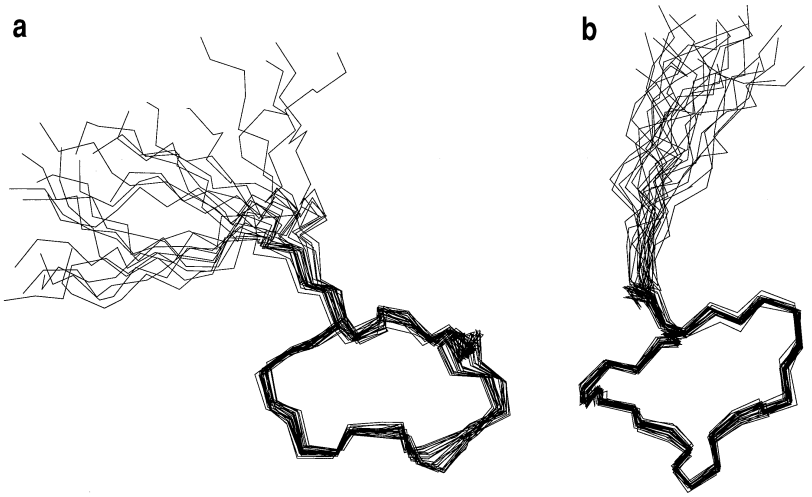

Fig. 3. Superposition of the backbone and fatty chain conformations obtained every 4 ps during the last 100 ps of MD simulation in water. (a) Class **I**; (b) class **II**.

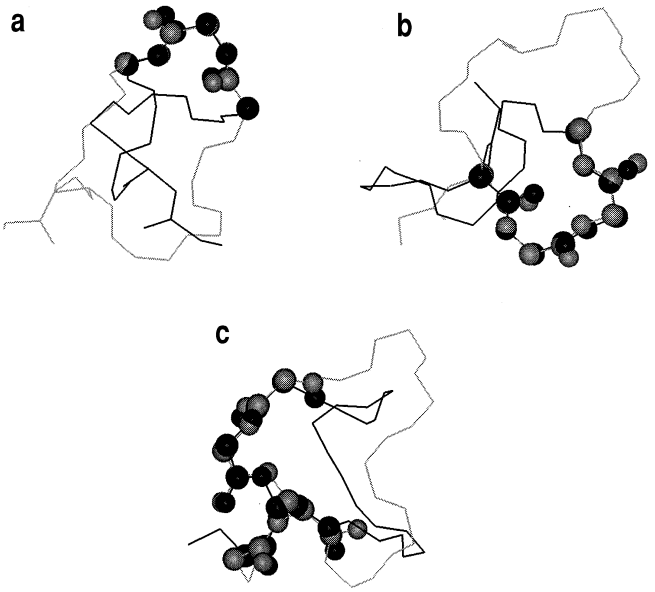

Fig. 4. Superposition of the conformationally comparable backbone regions of the average structures of classes I and II. (a) Region from C of A_2bu6 to N of Asp(OH)9. (b) Region from C^{α} of Ser2 to C^{α} of Lys5. (c) Region including the N-terminal Ser2 and the C-terminal Asp(OH)9 and *allo*-Thr(Cl)10 residues.

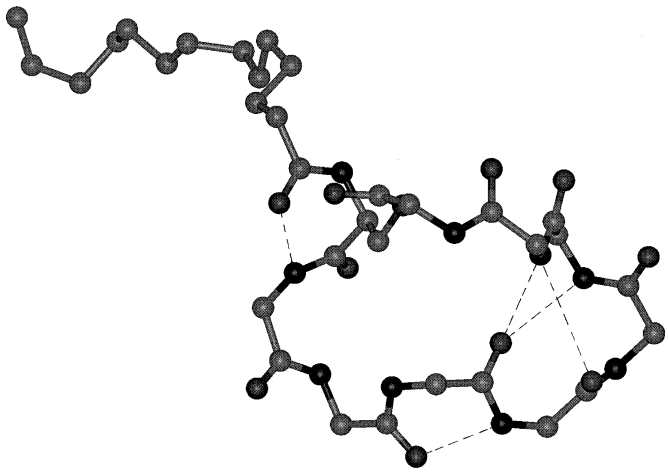

Fig. 5. Structure of PS-A obtained from MD simulations starting from the representative structure of class I. Hydrogen bonds are reported as dashed lines.

fluctuations of 4°, 8°, 9° and 19°, respectively. This β turn corresponds to the one observed in conformer **I**; however, they are of a different type, the former being of III′ type, although ϕ_i, ψ_i, ϕ_{i+1}, ψ_{i+1} dihedral angles somewhat deviate from the standard values (Rose et al., 1985). Another β turn, with an occurrence time of 94% is stabilised by a hydrogen bond between CO of Lys5 and NH of Dhb8. It has ϕ/ψ dihedral angles with average values of $\phi_6 = 54°$, $\psi_6 = 33°$, $\phi_7 = 37°$ and $\psi_7 = 46°$ and rms fluctuations of 5°, 5°, 4° and 8°, respectively. This β turn corresponds to that observed for conformer **I**, but also in this case of different type, being of type III′, although ϕ_i, ψ_i, ϕ_{i+1}, ψ_{i+1} dihedral angles somewhat deviate from the standard values (Rose et al., 1985). Another β turn is stabilised by a hydrogen bond between CO of Ser2 and NH of Lys5, with average dihedral ϕ_3, ψ_3, ϕ_4, ψ_4 angles of 67°, −100°, −85° and −15° and rms fluctuations of 5°, 10°, 9° and 11°, respectively. This turn can be classified as a II′ β turn.

No appreciable temporal changes in the values of ϕ/ψ angles were observed in the molecular dynamics trajectory. This imparts some higher conformational rigidity to the whole backbone ring of the class-**II** structure relative to the class-**I** structure. The superposition of the conformations obtained every 4 ps is reported in Fig. 3b.

An examination of the resulting structures shows that the two classes have three backbone regions which are comparable with respect to conformation. The first one extends from C^{α} of A_2bu6 to C^{α} of Dhb8, as shown in (Fig. 4a). The rmsd of backbone atoms C^{α}, N, C in residues, between the average class-**I** structure and the average class-**II** structure, is 0.05 ± 0.02 nm. The second one extends from C^{α} of Ser2 to C^{α} of Lys5, as shown in Fig. 4b. The rmsd of backbone atoms C^{α}, N, C, O in residues, between the average class-**I** structure and the average class-**II** structure, is 0.04 ± 0.03 nm. The third region includes the N-terminal Ser2 and the C-terminal Asp(OH)9 and *allo*-Thr(Cl)10 residues involved in the lactonic ring closure (Fig. 4c). The rmsd of backbone atoms C^{α}, N, C in residues, atoms C^{β} and O^{γ} of Ser and C1, C2 of fatty acid, between the average class-**I** structure and the average class-**II** structure, is 0.05 ± 0.02 nm.

A few backbone ϕ/ψ dihedral angles vary markedly between class-**I** and class-**II** structures. These are ϕ_2, ψ_5, ψ_5, ψ_6, ϕ_8 and

ϕ_9 and are responsible for the overall shape difference between the two structures.

The fatty chain in both classes is almost flexible, in agreement with the observation of only one contact involving the fatty chain, namely with Ser2.

In Fig. 5 the conformation of the class-**I** structure, which better corresponds than the class-**II** structure to the experimental NMR data, is shown.

DISCUSSION

Knowledge of the conformation in solution of bioactive substances that interact with biological membranes is an important requirement for the interpretation of their mode of action at the molecular level. The present paper reports the three-dimensional solution structure of Pseudomycin A, a bacterial amphiphilic lipodepsinonapeptide which belongs to a family of compounds affecting several membrane functions in plants (Iacobellis et al., 1992; Di Giorgio et al., 1994, 1996a, b, 1997; Camoni et al., 1995). The solution structure was elucidated by computer molecular simulations applying both DG and MD methods with the use of NOE data collected from fully assigned 2D NMR spectra (Ballio et al., 1994a). Classes **I** and **II** of conformers were obtained from the simulations. Class-**I** showed conformers that corresponded better to the NMR data. While the 2,3-dihydroxy fatty acyl is substantially unstructured, as previously found for some related products (Ballio et al., 1994b, 1995), the 28-membered peptide cycle is notable for its content of some secondary-structure elements joined to mobile hinges.

The overall three-dimensional structure in solution of Pseudomycin A is probably conditioned by two peculiar features of the molecule: the presence of a Dhb acid residue, which confers some conformational rigidity to the peptide chain, and the alternation of chiralities, which produces a conformational preference for turns (Wilmot and Thornton, 1988).

Similarly to Syringotoxin, Pseudomycin A shows a ring conformation which resembles the seam of a tennis ball, found for the first time in the bioactive lipodepsinonapeptide WLIP, produced by *Pseudomonas. reactans* (Mortishire-Smith et al., 1991).

An interaction of Pseudomycin A with biological membranes is suggested by the striking similarity of its activities (Iacobellis et al., 1992; Di Giorgio et al., 1994, 1997) with those of other natural peptides which affect the integrity of natural and artificial membranes (Saberwal and Nagaraj, 1994). Specific studies demonstrated that Syringomycin E and Syringopeptins 22A, 22B and 25A act like biosurfactant or ion-channel-forming compounds on biological membranes (Hutchinson et al., 1995; Hutchinson and Gross, 1997) and phospholipid bilayers (Camoni et al., 1995; Feigin et al., 1996, 1997). It is likely that the lipophilic character of Pseudomycin A, resulting from the presence of the fatty acid tail, is the prerequisite for this interaction. The likely association of the cationic cyclic region with the anionic head groups of the phospholipids might further favour this interaction.

This work has been supported in part by grants from the Ministero dell'Universita' e della Ricerca Scientifica e Tecnologica (MURST): Project 'Structural Biology', by the following grants of the Italian National Research Council (CNR): Special program 'Chimica fine II', Strategic Project 'Structural biology' and contract 95.02859, and by the EEC grant ERBFMRX-CT96-0013.

REFERENCES

Ballio, A., Bossa, F., Collina, A., Gallo, M., Iacobellis, N. S., Paci, M., Pucci, P., Scaloni, A., Segre, A. & Simmaco, M. (1990) Structure of Syringotoxin, a bioactive metabolite of *Pseudomonas syringae* pv. *syringae*, *FEBS Lett. 269*, 377−380.

Ballio, A., Barra, D., Bossa, F., Collina, A., Grgurina, I., Marino, G., Moneti, G., Paci, M., Pucci, P., Segre, A. L. & Simmaco, M. (1991) Syringopeptins, new phytotoxic lipodepsipeptides of *Pseudomonas syringae* pv. *syringae*, *FEBS Lett. 291*, 109−112.

Ballio, A., Bossa, F., Di Giorgio, D., Ferranti, P., Paci, M., Pucci, P., Scaloni, A., Segre, A. & Strobel, G. A. (1994a) Novel bioactive lipodepsipeptides from *Pseudomonas syringae*: the Pseudomycins, *FEBS Lett. 355*, 96−100.

Ballio, A., Collina, A., Di Nola, A., Manetti, C., Paci, M. & Segre, A. (1994b) Determination of structure and conformation in solution of Syringotoxin, a lipodepsipeptide from *Pseudomonas syringae* pv. *syringae* by 2D NMR and molecular dynamics, *Struct. Chem. 5*, 43−50.

Ballio, A., Bossa, F., Di Giorgio, D., Di Nola, A., Manetti, C., Paci, M., Scaloni, A. & Segre, A. L. (1995) Solution conformation of the *Pseudomonas syringae* p.v. *syringae* phytotoxic lipodepsipeptide SP25-A: 2D NMR, distance geometry and molecular dynamics, *Eur. J. Biochem. 234*, 747−758.

Berendsen, H. J. C., Postma, J. P. M., van Gunsteren, W. F., Di Nola, A. & Haak, J. R. (1984) Molecular dynamics with coupling to an external bath, *J. Chem. Phys. 81*, 3684−3690.

Braunschweiler, L. & Ernst, R. R. (1983) Coherence transfer by isotropic mixing: application to proton correlation spectroscopy, *J. Magn. Reson. 53*, 521−528.

Brooks, C. L. III & Karplus, M. (1983) Deformable stochastic boundaries in molecular dynamics, *J. Chem. Phys. 79*, 6312−6325.

Brooks, R. B., Bruccoleri, R. E., Olafson, B. D., States, D. J., Swaminathan, S. & Karplus, M. (1983) CHARMM: a program for macromolecular energy, minimization and dynamics calculations, *J. Comput. Chem. 4*, 187−217.

Brooks, C. L. III, Brünger, A. T. & Karplus, M. (1985) Active site dynamics in protein molecules: a stochastic boundary molecular-dynamics approach, *Biopolymers 24*, 843−865.

Brünger, A. T., Brooks, C. L. III & Karplus, M. (1985) Active site dynamics of ribonuclease, *Proc. Natl Acad. Sci. USA*, 8458−8462.

Brünger, A. T. *X-PLOR 3.1 Manual* (1988) Yale University, New Heaven, CT.

Camoni, L., Di Giorgio, D., Marra, M., Aducci, P. & Ballio, A. (1995) *Pseudomonas syringae* pv. *syringae* phytotoxins reversibly inhibit the plasma membrane H^+ ATPase and disrupt unilamellar liposomes, *Biochem. Biophys. Res. Commun. 214*, 118−124.

Di Giorgio, D., Camoni, L. & Ballio, A. (1994) Toxins of *Pseudomonas syringae* pv. *syringae* affect H^+-transport across the plasma membrane of maize, *Physiol. Plant 91*, 741−746.

Di Giorgio, D., Lavermicocca, P., Marchiafava, C., Camoni, L., Surico, G. & Ballio, A. (1996a) Effect of Syringomycin-E and Syringopeptins on isolated plant mitochondria, *Physiol. Mol. Plant Pathol. 48*, 325−334.

Di Giorgio, D., Camoni, L., Mott, K. A., Takemoto, J. Y. & Ballio, A. (1996b) Syringopeptins, *Pseudomonas syringae* pv. *syringae* phytotoxins resemble Syringomycin in closing stomata, *Plant Pathol. 45*, 564−571.

Di Giorgio, D., Camoni, L., Marchiafava, C. & Ballio, A. (1997) Biological activities of Pseudomycin A a lipodepsinonapeptide from *Pseudomonas syringae* MSU16H, *Phytochemistry 45*, 1385−1391.

Feigin, A. M., Takemoto, J. Y., Wangspa, R., Teeter, J. H. & Brand, J. G. (1996) Properties of voltage-gated ion channnel formed by Syringomycin E in planar lipid bilayers, *J. Membrane Biol. 149*, 41−47.

Feigin, A. M., Schagina, L. V., Takemoto, J. Y., Teeter, J. H. & Brand, J. G. (1997) The effect of sterols on the sensitivity of membranes to the channel-forming antifungal antibiotic, Syringomycin E, *Biochim. Biophys. Acta 1324*, 102−110.

Fukuchi, N., Isogai, A., Nakayama, J. & Suzuki, A. (1990a) Structure of Syringotoxin B, a phytotoxin produced by Citrus isolates of *Pseudomonas syringae* pv. *syringae*, *Agric. Biol. Chem. 54*, 3377−3379.

Fukuchi, N., Isogai, A., Yamashita, S., Suyama, K., Takemoto, J. Y. & Suzuki, A. (1990b) Structure of phytotoxin Syringomycin produced by a sugar cane isolate of *Pseudomonas syringae* pv. *syringae*, *Tetrahedron Lett. 31*, 1589−1592.

Gross, K.-H. & Kalbitzer, H. R. (1988) Distribution of chemical shifts in ^{1}H nuclear magnetic resonance spectra of proteins, *J. Magn. Reson. 76*, 87−89.

Harrison, L. A., Teplow, D. B., Rinaldi, M. & Strobel, G. A. (1991) Pseudomycins, a family of novel peptides from *Pseudomonas syringae* possessing broad-spectrum antifungal activity, *J. Gen. Microbiol. 137*, 2857−2865.

Hutchinson, M. L., Tester, M. A. & Gross, D. C. (1995) Role of biosurfactant and channel-forming activities of Syringomycin in transmembrane ion flux: a model for the mechanism of action in the plant pathogenic interaction, *Mol. Plant-Microbe Interact. 8*, 610−620.

Hutchinson, M. L. & Gross, D. C. (1997) Lipopeptide phytotoxins produced by *Pseudomonas syringae* pv. *syringae*: comparison of the biosurfactant and ion-channel-forming activities of Syringopeptin and Syringomycin, *Mol. Plant-Microbe Interact. 10*, 347−353.

Iacobellis, N. S., Lavermicocca, P., Grgurina, I., Simmaco, M. & Ballio, A. (1992) Phytotoxic properties of *Pseudomonas syringae* pv. *syringae* toxins, *Physiol. Mol. Plant-Pathol. 40*, 107−116.

Isogai, A., Fukuchi, N., Yamashita, S., Suyama, Y. & Suzuki, A. (1990) Structure of Syringostatin A and Syringostatin B novel phytotoxins produced by *Pseudomonas syringae* pv. *syringae* isolated from lilac blights, *Tetrahedron Lett. 31*, 695−698.

Jorgensen, W., Chandrasekar, J., Madura, J., Impey, R. & Klein, M. (1983) Comparison of simple potential functions for simulating liquid water, *J. Chem. Phys. 79*, 926−935.

Kaptein, R., Boelens, R., Scheek, R. M. & Gunsteren, W. F. (1988) Protein Structures from NMR, *Biochemistry 27*, 5389−5395.

Kirkpatrick, S., Gelatt, C. D. Jr & Vecchi, M. P. (1983) Optimization by simulated annealing, *Science 220*, 671−680.

Lam, B. S., Strobel, G. A., Harrison, L. A. & Lam, S. T. (1987) Transposon mutagenesis and tagging of fluorescent *Pseudomonas*: antimycotic production is necessary for control of Dutch elm disease, *Proc. Natl Acad. Sci. USA 84*, 6447−6451.

MacKerell, A. D. Jr, Bashford, D., Bellott, M., Dunbrack, R. L. Jr, Field, M. J., Fischer, S., Gao, J., Guo, H., Ha, S., Joseph, D., Kuchnir, L., Kuczera, K., Lau, F. T. K., Mattos, C., Michnick, S., Ngo, T., Nguyen, D. T., Prodhom, B., Roux, B., Schlenkrich, M., Smith, J. C., Stote, R., Straub, J., Wiorkiewicz-Kuczera, J. & Karplus, M. (1992) Self consistent parametrization of biomolecules for molecular modeling and condensed phase simulations, *FASEB J. 6*, A143.

Marion, D. & Wüthrich, K. (1983) Application of phase sensitive two-dimensional correlated spectroscopy (COSY) for measurements of ^{1}H-^{1}H spin−spin coupling constants in proteins, *Biochem. Biophys. Res. Commun. 113*, 967−974.

Mortishire-Smith, R. J., Nutkins, J. C., Packman, L. C., Brodey, C. L., Rainey, P. B., Johnstone, K. & Williams, D. H. (1991) Determination of the structure of an extracellular peptide produced by the mushroom saprotroph *Pseudomonas reactans*, *Tetrahedron 47*, 3645−3654.

Nilges, M., Clore, M. G. & Gronenborn, A. M. (1988) Determination of three-dimensional structures of proteins from interproton distance data by hybrid distance geometry-dynamical simulated annealing calculations, *FEBS Lett. 229*, 317−324.

Powell, M. J. D. (1977) Restart procedures for the conjugate gradient method, *Mathematical Programming 12*, 241−254.

Rose, G. D., Gierasch, L. M. & Smith J. A. (1985) Turns in peptides and proteins, *Adv. Prot. Chem. 37*, 1−109.

Roux, M. (1985) *Algorithmes de classification*, Masson, Paris.

Ryckaert, J. P., Ciccotti, G. & Berendsen, H. J. C. (1977) Algorithms for macromolecular dynamics and constraint dynamics, *Mol. Phys. 34*, 1311−1327.

Saberwal, G. & Nagaraj, R. (1994) Cell-lytic and antibacterial peptides that act by perturbing the barrier function of membranes: facets of their conformational features, structure−function correlations and membrane-perturbing abilities, *Biochim. Biophys. Acta 1197*, 109−131.

Segre, A. L., Bachmann, R. C., Ballio, A., Bossa, F., Grgurina, I., Iacobellis, N. S., Marino, G., Pucci, P., Simmaco, M. & Takemoto, J. Y. (1989) The structure of Syringomycins A1, E and G, *FEBS Lett. 255*, 27−31.

Thioulouse, J. (1989) Statistical analysis and graphical display of multivariate data on the Macintosh, *Comput. Appl. Biosci. 5*, 287−292.

Wagner, G., Braun, W., Havel, T. F., Schaumann, T., Go, N. & Wüthrich, K. (1987) Protein structure in solution by nuclear magnetic resonance and distance geometry. The polypeptide fold of the basic pancreatic trypsin inhibitor determined using two different algorithms, DISGEO and DISMAN, *J. Mol. Biol. 196*, 611−640.

Wilmot, C. M. & Thornton, J. M. (1988) Analysis and prediction of different types of β turns in proteins, *J. Mol. Biol. 203*, 221−232.